crystals

MDPI

Article

Numerical Simulations of Circular Dichroism and Polarization Conversion in VO_2-Based Terahertz Metamaterials

Gui Jin [1], Yi Ren [2] and Bin Tang [2,*]

[1] Department of Electronic Information and Electronic Engineering, Xiangnan University, Chenzhou 423000, China
[2] School of Microelectronics and Control Engineering, Changzhou University, Changzhou 213163, China
* Correspondence: btang@cczu.educn

Abstract: Metamaterials with actively tunable functionalities are highly desirable for applications of advanced optoelectronic devices. In this paper, we theoretically present a metamaterial with diversified functionalities by availing of the phase transition characteristics of vanadium dioxide (VO_2) in terahertz frequency regions. The research results demonstrate that the function of the designed metamaterial can be switched from giant circular dichroism (CD) to a reflecting broadband half-wave plate (HWP) and a quarter-wave plate (QWP). When VO_2 is in the isolating state, the metamaterial exhibits a quite distinct transmission efficiency for circularly polarized lights, thus resulting in a maximum CD value ~0.97 at the resonant frequency. When VO_2 is operating in the metallic state, the metamaterial performs like a broadband HWP, in which the nearly perfect linear polarization conversion can be achieved at the frequency range from 3 to 7 THz. Moreover, the structure can play a role of a high-efficiency QWP that can simultaneously convert the incident linear polarized light to left-handed and right-handed circularly polarized light. The calculated ellipticity indicates a good polarization conversion at the frequency of 2.4 THz and 7.4 THz, respectively. The physical mechanism of the discussed features and effects can be explained by exploring the electric field distributions. Furthermore, the structural parameters also exert great influences for achieving giant CD and HWP as well as QWP. The proposed metamaterial may offer a new approach for designing metamaterial devices with multi-functions in THz regions.

Keywords: metamaterials; circular dichroism; polarization conversion; vanadium dioxide (VO_2)

check for updates

Citation: Jin, G.; Ren, Y.; Tang, B. Numerical Simulations of Circular Dichroism and Polarization Conversion in VO_2-Based Terahertz Metamaterials. *Crystals* **2023**, *13*, 437. https://doi.org/10.3390/cryst13030437

Academic Editor: Youngpak Lee

Received: 15 February 2023
Revised: 24 February 2023
Accepted: 28 February 2023
Published: 3 March 2023

Copyright: © 2023 by the authors. Licensee MDPI, Basel, Switzerland. This article is an open access article distributed under the terms and conditions of the Creative Commons Attribution (CC BY) license (https://creativecommons.org/licenses/by/4.0/).

1. Introduction

Circular dichroism (CD) [1,2], refers to the difference of light transmission, reflection or absorption efficiencies between left-handed circularly polarized (LCP) light and right-handed circularly polarized (RCP) light, which has attracted a growing amount of attention due to its wide applications [3,4]. However, the CD response obtained by utilizing natural materials is weak to detect. Therefore, extensive research works have been proposed to design and achieve the highest possible CD values in metamaterial-based nanostructures [5–9]. As for metamaterial [10], it is a kind of artificial material possessing exotic electromagnetic characteristics achieved by carefully constructing the structural units [11,12]. Over the past few years, amounts of functional optoelectronic devices have been proposed at the frequency ranges from the visible lights to terahertz (THz) waves [13,14]. It is also worth noting that terahertz waves have been widely utilized in imaging, photoelectric detection and spectroscopy in recent years. Furthermore, another significant application of terahertz metamaterial, polarization conversion [15], plays an important role in manipulating the polarization state of electromagnetic waves [16]. Generally, the half-wave plate (HWP) and quarter-wave plate (QWP) are two typical kinds of waveplates among the polarization optical components [17]. The HWP can rotate the azimuth of the polarized light at any arbitrary degree, and the QWP can convert linearly polarized light to circularly polarized and vice versa. In terahertz frequency regions, traditional wave plates are made of

birefringent materials, which usually work at a fixed single function or limited operating frequency bandwidth.

In practical applications, photonics devices with actively tunable functionalities are highly desirable to be compatible with integrated metamaterials [18–22]. However, it is hard to realize tunable functionality for typical metamaterials consisting of precious metals and dielectric elements once the architecture is designed and fabricated. Thus, strategies have been proposed by integrating active materials with nanostructures, such as two-dimensional materials [23], semiconductors [24], etc. As alternative materials, phase change materials [25], e.g., vanadium dioxide (VO_2), has attracted much interest as its optoelectronic properties can go through dramatic change during phase transition at the critical temperature about 68 °C [26–29]. Recently, varieties of VO_2-based metamaterial nanostructures have been proposed to acquire multiple functions [30–36]. For example, Ding et al. theoretically suggested a VO_2-based metasurface which can achieve switchable functionalities between a broadband absorber and a reflecting HWP [37]. Luo et al. designed a metal-VO_2-assisted metamaterial which can be utilized as broadband terahertz HWP and QWP [38]. Very recently, Tang et al. proposed an actively tunable metamaterial device based on the hybrid VO_2–graphene integrated configuration [39], in which the switching between asymmetric transmission and polarization conversion can be achieved. However, as far as we know, there have been no reports of metamaterial devices that can switch between optical CD and HWP, as well as QWP in the terahertz range.

In this paper, we propose a metamaterial with diversified functionalities that can switch from giant CD to a reflecting broadband HWP and QWP by availing of insulator-to-metal transition in VO_2 in terahertz regions. When VO_2 is in the isolating state, the metamaterial exhibits distinct transmission efficiency for circularly polarized light, and a maximum value of CD exceeds 0.97 at the resonant frequency. When VO_2 is in the metallic state, the metamaterial acts as a broadband HWP, and the nearly perfect linear polarization conversion can be obtained at the frequency range from 3 to 7 THz. Moreover, the metamaterial can play a role of a high-efficiency QWP that can simultaneously convert the incident linear polarized light to left-handed and right-handed circularly polarized light, and the calculated ellipticity indicates a good polarization conversion at the frequency of 2.4 THz and 7.4 THz, respectively. The physical mechanism of the above phenomena can be explained by exploring the electric field distributions. Furthermore, the structural parameters also exert great influences for achieving giant CD and HWP as well as QWP. The proposed metamaterial may offer a new approach for developing nanophotonic devices with diversified functions in THz region.

2. Structural Design and Methods

Figure 1a depicts the polarization conversion function of designed metamaterial under the illumination of linearly polarized waves when VO_2 is in the metallic state. As illustrated in Figure 1b, the designed metamaterial is utilized to realize circular dichroism under the illumination of circularly polarized waves when VO_2 is in the isolating state. Figure 1c shows the schematic of a unit cell, which is composed of a Au strip, SiO_2, a Au split ring, VO_2, SiO_2 and a Au strip from top to bottom. The upper and bottom Au strips have the same rotation angle θ with respect to the y-axis. Figure 1d shows the side view of the designed metamaterial in the x-z plane. The optimized geometric parameters are listed in the caption of Figure 1. SiO_2 is selected as the dielectric layer, and the refractive index is 1.45. According to Drude model, the effective permittivities of VO_2 and Au at terahertz frequency can be expressed as follows [30]:

$$\varepsilon_{\mathrm{Au}}(\omega) = 1 - \frac{\omega_{p\mathrm{Au}}^2}{\omega^2 + i\gamma_{\mathrm{Au}}\omega} \tag{1}$$

$$\varepsilon_{\mathrm{VO_2}}(\omega) = \varepsilon_\infty - \frac{\omega_p^2(\sigma)}{\omega^2 + i\gamma_{\mathrm{VO_2}}\omega} \tag{2}$$

$$\omega_p^2(\sigma) = \frac{\sigma}{\sigma_0}\omega_p^2(\sigma_0) \tag{3}$$

where the plasma frequency $\omega_{p\mathrm{Au}}$ of Au is $1.37 \times 10^{16}\ rad/s$, the collision frequency γ_{Au} is $4.08 \times 10^{13}\ rad/s$. $\varepsilon_\infty = 12$ is the dielectric permittivity at the infinite frequency for VO_2, γ_{VO_2} is $5.75 \times 10^{13}\ rad/s$, $\omega_p(\sigma)$ is the plasma frequency based on conductivity σ, $\sigma_0 = 3 \times 10^5\ S/m$, $\omega_p(\sigma_0) = 1.4 \times 10^{15}\ rad/s$. In simulation, the conductivities of VO_2 in the metallic state is set as $3 \times 10^5\ S/m$, and the conductivities of VO_2 in the isolating state is set as $10\ S/m$. In this work, the three-dimensional finite-difference time-domain (FDTD) method was utilized to perform the electromagnetic simulations. The spatial mesh dimensions were set to $\Delta x = \Delta y = \Delta z = \Delta s = 5$ nm, and the time step was taken as $\Delta t = \Delta s/2c$ (c is the velocity of light in vacuum) and the total time step number was 2×10^5, which ensures that the electromagnetic fields were stable and convergent. The optimized geometric parameters are listed in the caption of Figure 1. To obtain the optimum values of the parameters, the parameter sweeps were made in simulations. The optimizations of these parameters were performed by altering the sizes and the positions of the elements, and the periodic boundaries were set in both the x and y directions, while in the z direction, perfectly matched layers were utilized.

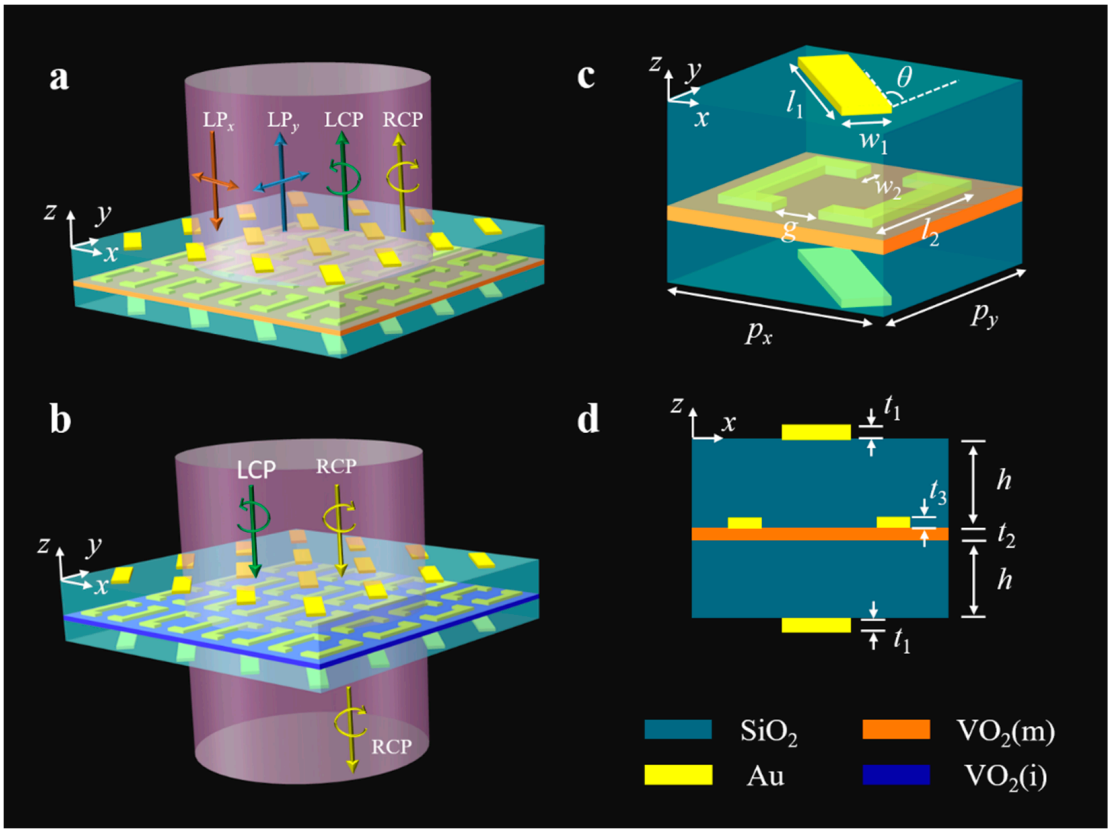


Figure 1. Schematic of the proposed metamaterial with 3×3 unit cells under x- and y-polarized waves when VO_2 is in the (**a**) metallic and (**b**) isolating states, respectively. (**c**) A unit cell of the proposed metamaterial. (**d**) The side view of the proposed structure in the x-z plane. The optimized geometric parameters are listed as below: $p_x = p_y = 20$ µm, $l_1 = 29$ µm, $l_2 = 24$ µm, $w_1 = 7$ µm, $w_2 = 4$ µm, $t_1 = 0.7$ µm, $t_2 = 0.7$ µm, $t_3 = 0.6$ µm, $g = 4$ µm, $h = 9.65$ µm.

Based on the polarization conversion theory, one can build a connection between the reflected electric fields and the incident electric field with a Jones matrix. The incident and reflected electric fields can be described as [34]:

$$E_i(r,t) = \begin{pmatrix} I_x \\ I_y \end{pmatrix} e^{i(kz-\omega t)} \tag{4}$$

$$E_r(r,t) = \begin{pmatrix} R_x \\ R_y \end{pmatrix} e^{i(kz-\omega t)} \tag{5}$$

where ω represents the angular frequency, k denotes the wave vector, and the complex amplitudes of the incident wave components in the x-and y-directions are represented by I_x and I_y, respectively. Similarly, the complex amplitudes of the reflected wave components in the x- and y-directions are represented by R_x and R_y, respectively. The complex amplitudes of the reflected light can be expressed as [38]:

$$\begin{pmatrix} R_x \\ R_y \end{pmatrix} = \begin{pmatrix} r_{xx} & r_{xy} \\ r_{yx} & r_{yy} \end{pmatrix} \begin{pmatrix} I_x \\ I_y \end{pmatrix} \tag{6}$$

The polarization conversion ratio (*PCR*) can be defined as the ratio of the power of the converted cross-polarized light and the total transmitted powers. Herein, *PCR* for linearly polarized lights can be calculated as [40]:

$$PCR(x) = \frac{|t_{yx}|^2}{|t_{xx}|_2+|t_{yx}|^2} = \frac{T_{yx}}{T_{xx}+T_{yx}} \tag{7}$$

$$PCR(y) = \frac{|t_{xy}|^2}{|t_{xy}|_2+|t_{yy}|^2} = \frac{T_{xy}}{T_{xy}+T_{yy}} \tag{8}$$

where $PCR(x)$ and $PCR(y)$ denote the polarization conversion ratio for x- and y-polarized lights, respectively. t_{ij} ($i(j) = x,y$) denotes i-polarized transmission coefficient from j-polarized incident lights, and $T_{ij} = |t_{ij}|^2$.

In addition, to quantify the efficiency of the linear-to-circular polarization conversion, the ellipticity (χ) can be defined as $\chi = S_3/S_0$, in which the Stokes parameters (S) are given by the following formulas [17]:

$$S_0 = |r_{xx}|_2+|r_{yx}|^2 \tag{9}$$

$$S_1 = |r_{xx}|_2-|r_{yx}|^2 \tag{10}$$

$$S_2 = 2|r_{xx}||r_{yx}|\cos(\Delta\Phi) \tag{11}$$

$$S_3 = 2|r_{xx}||r_{yx}|\sin(\Delta\Phi) \tag{12}$$

where $\Delta\Phi$ represents the phase difference between two orthogonal polarizations.

3. Results and Discussion

When VO_2 is in the isolating state, the substrate enables the optical transmission of incident lights along the forward (-z) direction. Figure 2a shows the calculated optical transmission spectra for the designed metamaterial when illuminated by circularly polarized lights. One can clearly see from Figure 2a that the optical responses exhibit distinct transmission efficiencies for both circularly polarized lights. Specifically, there exists an obvious transmission resonant peak at the frequency of 2.95 THz for the illumination of RCP light. By contrast, there appears a transmission dip at the same frequency for the illumination of LCP light. As a result, the circular dichroism (CD) response can be achieved according to the difference in transmittance between LCP and RCP light illuminations [1], which can be calculated by the formula CD = $T_{RCP} - T_{LCP}$. The corresponding optical

CD spectrum is given in Figure 2b, in which the maximum value of CD exceeds 0.97 at the frequency of 2.95 THz. To understand the operation mechanism of CD, Figure 2c,d illustrate the electric field distributions at x-z plane when illuminated by RCP and LCP lights, respectively. One can obviously find from Figure 2c that a strong electric field is excited at the resonant frequency of 2.95 THz in each part of Au nanostructure. Thus, most of the radiative photons can be emitted out of the structure under the illumination of RCP light. However, the excited electric field in the corresponding part of Au nanostructure becomes much weaker under LCP illumination, as depicted in Figure 2d. As a result, most of the incident photon energies are reflected due to the scattering effect occurring in the split ring. Therefore, a strong CD response can be achieved when VO_2 is in the isolating state.

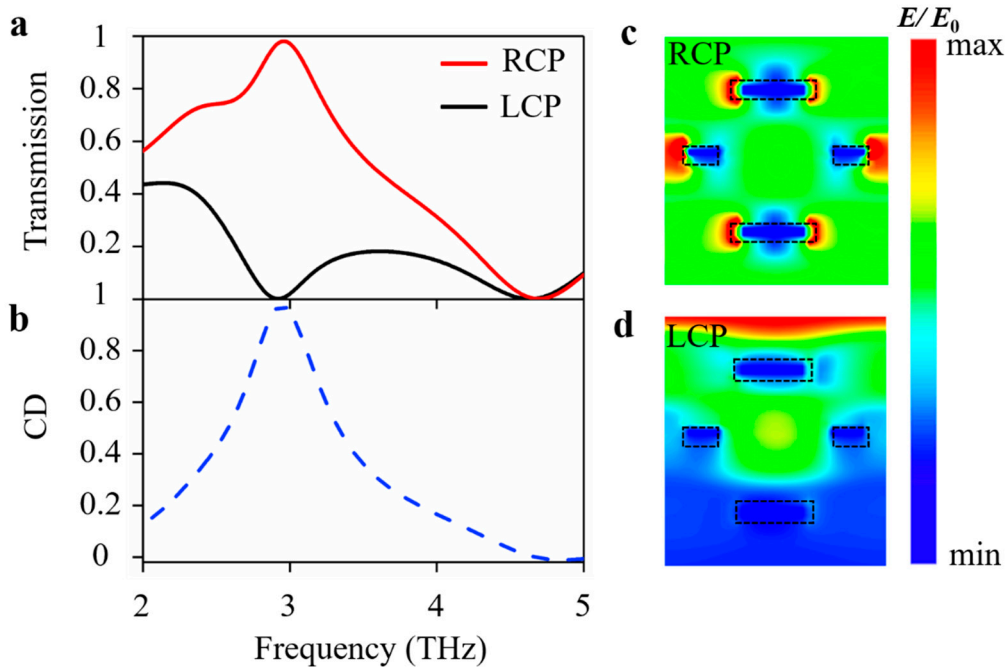


Figure 2. (**a**) The calculated transmission spectra of the proposed metamaterial and (**b**) the corresponding CD response for circularly polarized lights when VO_2 is in the isolating state. The side views of the electric field distributions for (**c**) RCP light and (**d**) LCP light at the resonant frequency of 2.95 THz, respectively.

When VO_2 is transformed from dielectric state to the metallic state, the VO_2 film serves as a metal background that blocks the light transmission. Figure 3a depicts the reflection amplitude components of forward propagating light with x-polarization. One can find that R_{yx} and R_{xx} show a great discrepancy across the operating frequency range, indicating that the incident x-polarized light is almost converted into y-polarized light. Moreover, the total reflected power reaches over 90% at the frequency range from 3 to 7 THz, manifesting that the designed metamaterial can act as an HWP. Figure 3b illustrates the spectra of two reflection phases and the corresponding phase difference $\Delta\Phi$ between two reflection phases. It is obviously that the phase difference $\Delta\Phi$ goes through great change from $\sim -\pi/2$ to $\sim 3\pi/2$ across the whole frequency range. Figure 3c depicts the PCR spectra for forward incident x-polarized light, where nearly perfect linear polarization conversion can be obtained at the frequency range from 3 to 7 THz. Figure 3d shows the calculated ellipticity spectra for forward incident x-polarized light. According to the definition of ellipticity (χ), it indicates a perfect LCP light when the ellipticity $\chi = 1$, and a perfect RCP light when $\chi = -1$. In particular, it should be noted that the linear-to-circular polarization conversion can be achieved if the reflection amplitudes satisfy the relationships as follows: $R_{xx} = R_{yx}$ and $\Delta\Phi = \Phi_{yx} - \Phi_{xx} = 2m\pi \pm \pi/2$, where m is an integer, and "+" and "−" manifest the RCP and LCP lights. Based on the above, one can find that perfect

linear-to-circular polarization conversion can be achieved for the proposed structure at the frequency of 2.4 THz and 7.4 THz, respectively. That is to say, the metamaterial device serves as a QWP which can transform the incident *x*-polarized light into reflected RCP and LCP lights. Therefore, the designed device can simultaneously play the role of HWP and QWP at different working frequencies when VO_2 is in the metallic state.

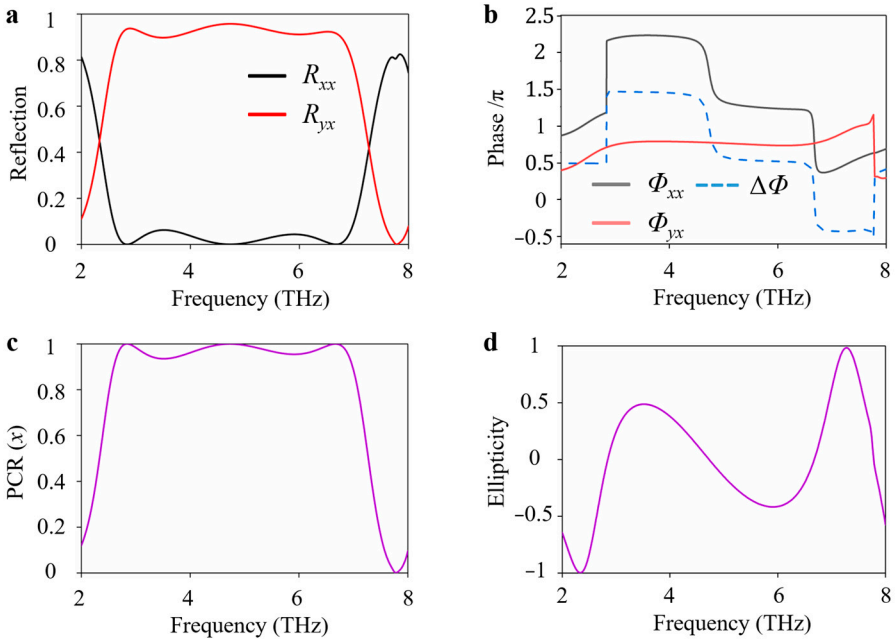


Figure 3. (**a**) The reflection spectra of forward illuminated *x*-polarized light when VO_2 is in the metallic state. (**b**) The spectra of the phase and the calculated phase difference of the two reflection coefficients. (**c**) The PCR spectra for forward incident *x*-polarized light, and (**d**) the calculated ellipticity spectra.

In addition, it is worth noting that the geometrical parameter, i.e., the rotation angle θ, has great influences on the optical responses and polarization conversion. When VO_2 is in the isolating state, Figure 4 depicts the calculated optical transmission spectra and CD responses as a function of the rotation angle and wavelength under the illumination of LCP and RCP lights, respectively. It can be seen that with the increase of θ, the transmission efficiency exhibits huge differences for both polarizations and the optical CD responses go through dramatic changes. When the rotation angle θ is fixed at 0°, the transmission efficiency for RCP and LCP lights is nearly same, thus the calculated CD response is near zero. In particular, one can clearly find from Figure 4a that with the increase of the rotation angle from 15° to 75°, the resonant dip of the optical transmission spectra for the illumination of LCP light takes on a low value and shows a blueshift at the frequency range from 2.5 to 3.4 THz. Meanwhile, as shown in Figure 4b, the resonant peak of the optical transmission spectra for the illumination of RCP light keeps a high value and also displays a blueshift at the corresponding frequency range. Therefore, the optical CD responses calculated in Figure 4c remain over 0.9 at the resonant frequency when the rotation angle θ increases from 15° to 75°. This can be attributed to that the chirality of the structural changes when the rotation angle θ is altered.

When VO_2 acts as a metal, the polarization conversions are calculated in Figure 5 for the designed metamaterial device with different rotation angles θ. Figure 5a,b depict the reflection amplitude components R_{xx} and R_{yx} of the *x*-polarized light propagating along the forward direction, respectively. One can find that R_{xx} remains at low values whereas R_{yx} remains at high values when the rotation angle θ increases from 30° to 60° at the operating frequency range from 2.3 to 6.5 THz, indicating that the significant polarization conversion occurs for the incident *x*-polarized light. The corresponding PCR spectra are illustrated in

Figure 5c, in which the maximum PCR reaches over 99.9% at the frequency range from 2.3 to 6.5 THz. Figure 5d shows the calculated ellipticity with various rotation angles θ. It can be found that the calculated ellipticity maintains the maximum and minimum values at the corresponding frequency peak when the rotation angle θ increases from 30° to 60°.

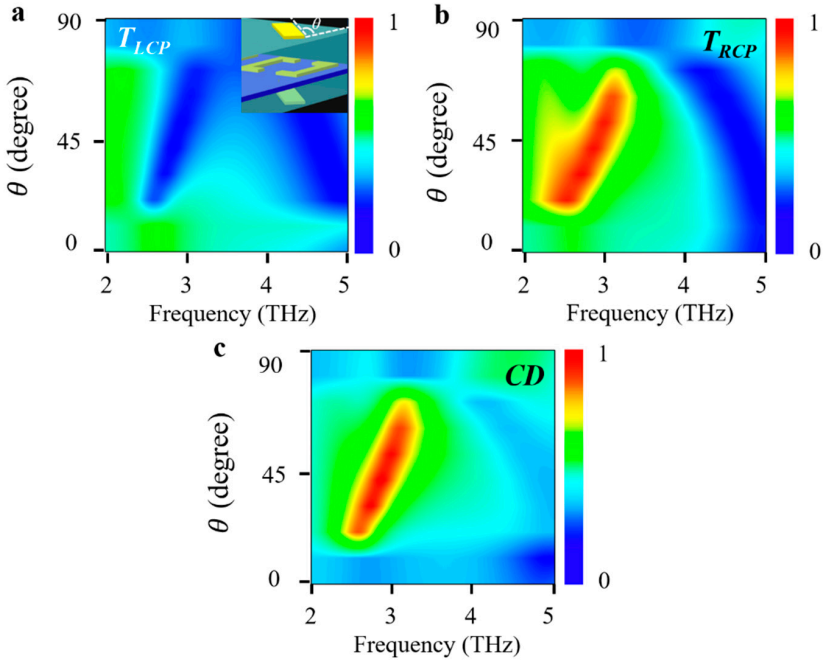


Figure 4. The transmission spectra versus different rotation angles θ for the illumination of (**a**) RCP light and (**b**) LCP light. (**c**) The corresponding CD response spectra versus different rotation angles θ. The inset in (**a**) depicts the related geometric parameter and VO_2 is in the isolating state.

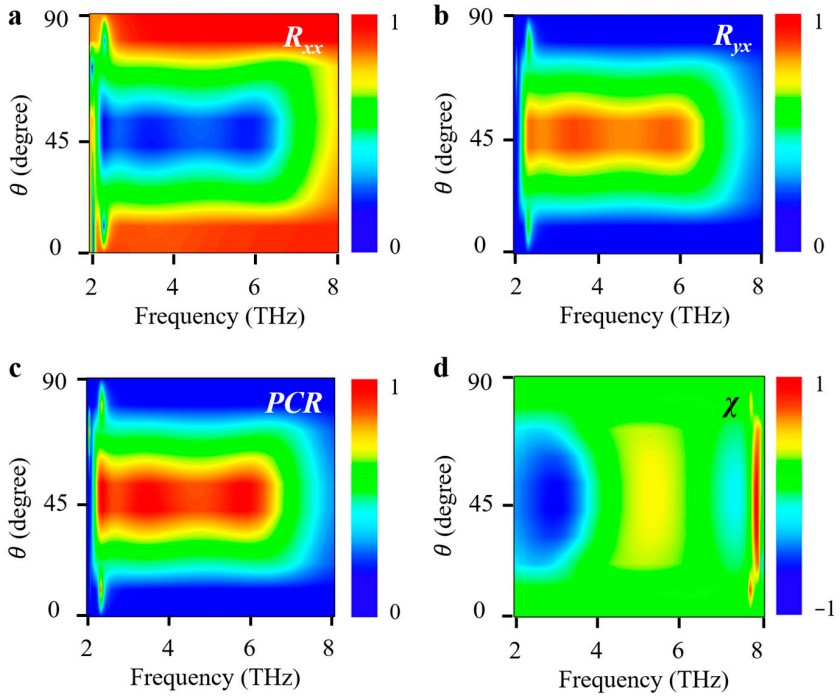


Figure 5. (**a**,**b**) The spectra of reflection coefficients for forward illumination of x-polarized lights for various rotation angles θ. (**c**) The calculated PCR (x) spectra and (**d**) ellipticity spectra of x-polarized lights for various rotation angles θ. VO_2 is in the metallic state.

Next, we will discuss the influences of the dielectric layer thickness h on the optical CD response and polarization conversion ratio for the designed metamaterial device when VO_2 is in the isolating state. Figure 6a,b show the optical transmission spectra versus different h under the illumination of LCP and RCP lights, respectively. Comparing Figure 6a,b, the optical spectra exhibit huge difference near the resonant frequency of 3 THz due to the different transmission efficiencies for both polarizations. One can clearly find that with the increase of h, the resonant dip of optical transmission for the illumination of LCP light always maintains a low value. Meanwhile, the resonant peak of optical transmission for the illumination of RCP light shows a high transmission efficiency and has a slight redshift. Therefore, the calculated CD responses reach over 0.9 when the height h increases from 4 to 10 μm, as depicted in Figure 6c.

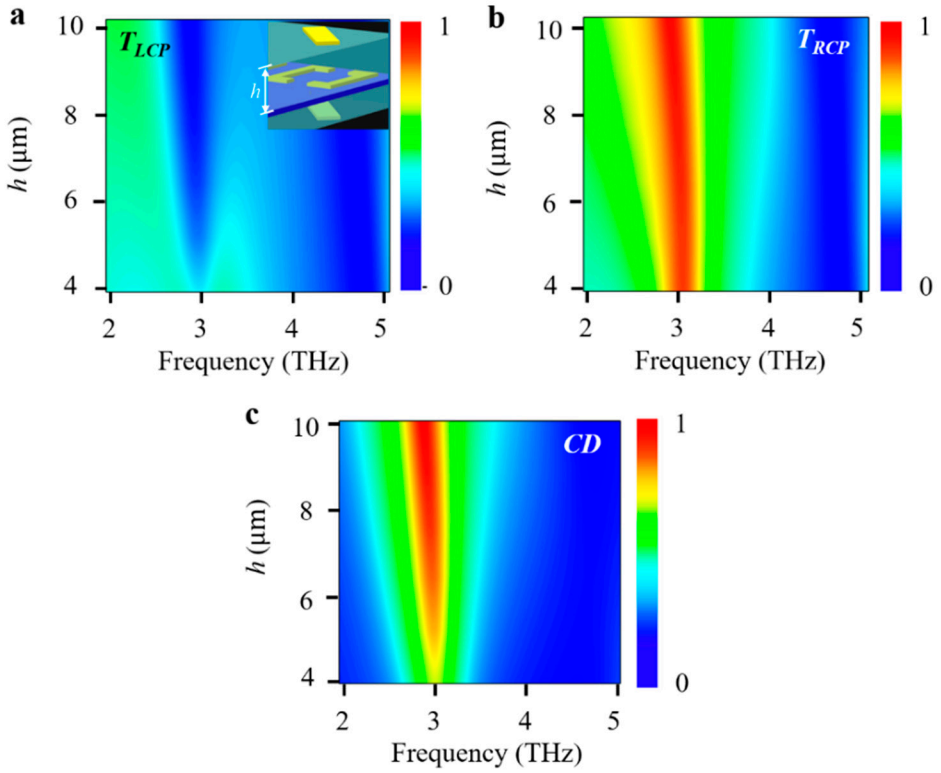


Figure 6. The calculated transmission spectra versus height h for the illumination of (**a**) LCP light and (**b**) RCP light. (**c**) The calculated corresponding CD response spectra versus different height h. The inset in (**a**) depicts the related geometric parameter and VO_2 is in the isolating state.

When VO_2 is in the metallic state, the polarization conversions are studied for the designed metamaterial device with different h. Figure 7a,b depict the reflection amplitude components R_{xx} and R_{yx} of the forward propagation for x-polarized lights, respectively. One can find from Figure 7a,b that the dielectric layer thickness h has an obvious effect on the reflection amplitude components R_{xx} and R_{yx}. When the dielectric layer thickness h takes a small value, i.e., h = 4 μm, the incident x-polarized light is partially converted into y-polarized light. With the further increasing of h, the polarization conversion efficiency is improved gradually. Correspondingly, the PCR spectra undergo a change from dual-band to broadband, as indicated in Figure 7c, in which the maximum PCR value reaches over 99.9% at the frequency range from 2.3 THz to 6.2 THz, indicating that the significant polarization conversion occurs for the incident x-polarized light. Meanwhile, the calculated ellipticity for forward propagated x-polarization light is depicted in Figure 7d. It can be found that the calculated ellipticity maintains the maximum and minimum values at the corresponding frequency peak except for a redshift. Moreover, the frequency regions of

the converted LCP gradually become narrow while the frequency regions of the converted RCP gradually become broad.

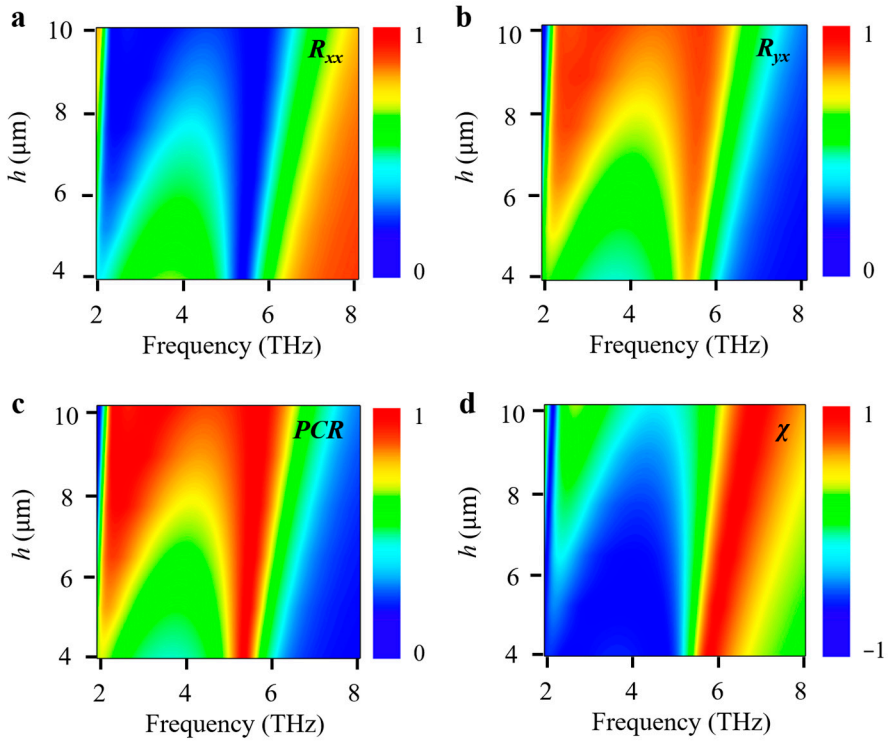


Figure 7. (**a**,**b**) The spectra of reflection coefficients for forward illuminated *x*-polarized light for various height *h*. (**c**) The calculated PCR (*x*) spectra, and (**d**) ellipticity spectra of *x*-polarized light for various height *h*. VO_2 is in the metallic state.

Finally, the changes of gap distance *g* of the Au split ring are investigated since it is a vital factor which can highly affect the CD response and polarization conversion ratio. When VO_2 is in the isolating state, the transmission efficiency is calculated for the designed metamaterial device with different gap distances *g*. Figure 8a,b show the optical transmission spectra versus different gap distances *g* under the illumination of LCP and RCP lights, respectively. From Figure 8a,b, one can find that the transmission efficiency exhibits huge difference with the increase of *g*. The resonant dip of optical transmission for the illumination of LCP light always maintains a low value and shows a blueshift as the gap distance *g* increases gradually from 4 μm to 12 μm. By contrast, the resonant peak of optical transmission for the illumination of RCP light maintains a high value, especially when $g > 5$ μm, thus resulting in the optical CD responses depicted in Figure 8c.

When VO_2 is in the metallic state, the polarization conversion for the designed metamaterial device with different gap distances are graphically illuminated in Figure 9. Figure 9a,b depict the reflection amplitude components R_{xx} and R_{yx} of the forward propagated *x*-polarization lights, respectively, when the gap distance *g* increases from 4 to 12 μm. One can find that R_{xx} remains at nearly zero, whereas R_{yx} reaches up to 1 at the frequency range from 2.3 to 6.2 THz, indicating that the significant polarization conversion occurs for the incident *x*-polarized lights. The corresponding PCR spectra are illustrated in Figure 9c, in which the PCR values remain over 99% in the above frequency range. In addition, it can be seen in Figure 9d that the calculated ellipticity reaches the maximum value (+1) and minimum value (−1) at the corresponding frequency peak apart from a redshift. Moreover, the frequency regions of the converted LCP lights gradually become narrow, while the frequency regions of the converted RCP lights gradually become broad with the increase in *g*.

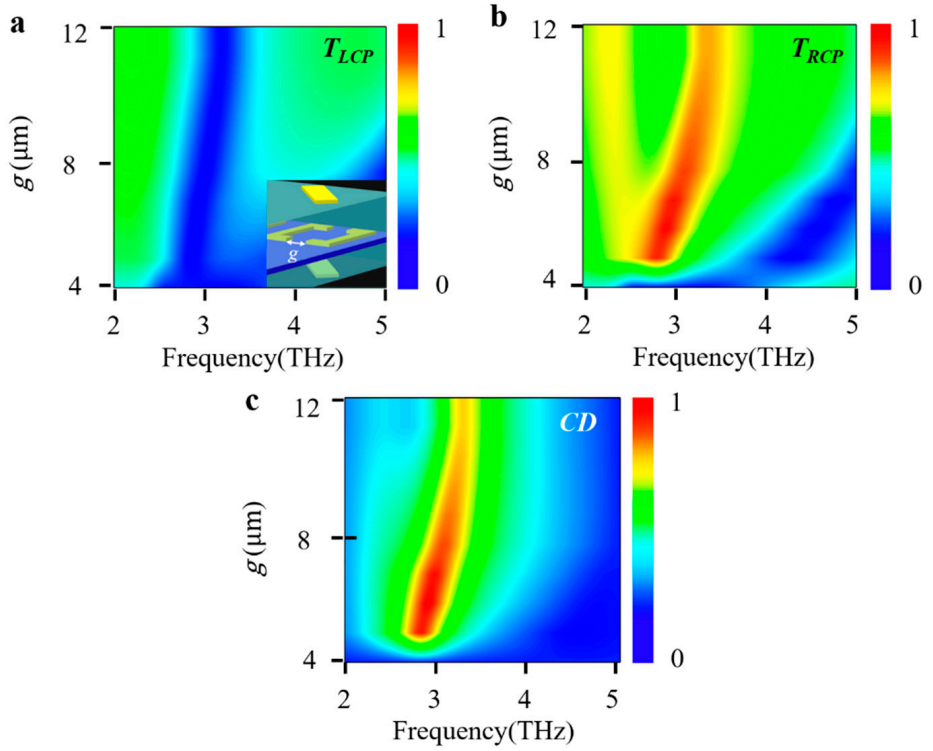


Figure 8. The calculated transmission spectra versus gap distances g for the illumination of (**a**) RCP light and (**b**) LCP light. (**c**) The calculated corresponding CD response spectra versus different gap distances g. The inset in (**a**) depicts the related geometric parameter and VO_2 is in the isolating state.

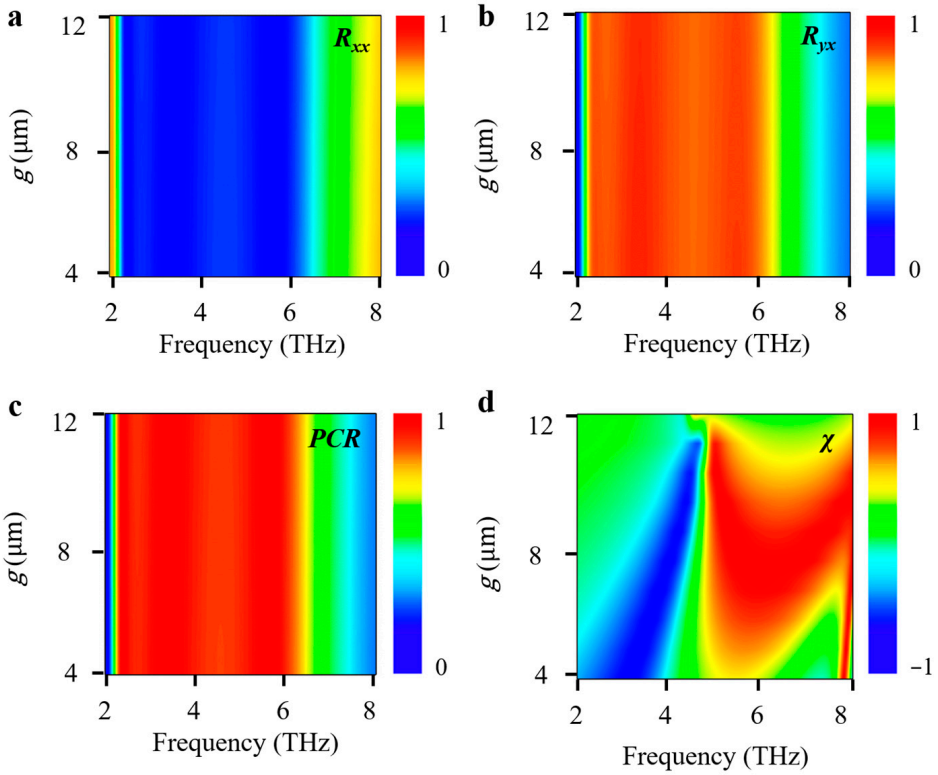


Figure 9. (**a**,**b**) The spectra of reflection coefficients for forward illuminated x-polarized light for various gap distances g. (**c**) The calculated PCR (x) spectra, and (**d**) ellipticity spectra of x-polarized light for various gap distances g. VO_2 is in the metallic state.

4. Conclusions

In this paper, we theoretically propose a metamaterial device with diversified functionalities by availing of the insulator-to-metal transition in VO_2 at THz frequencies. The simulated results indicate that the designed metamaterial can transition from having a giant circular dichroism function to exhibiting reflective broadband behavior as a half-wave plate (HWP) and quarter-wave plate (QWP). When VO_2 is in the isolating state, the metamaterial exhibits distinct transmission efficiency for circularly polarized lights, and the maximum value of CD exceeds 0.97 at the resonant frequency of 2.95 THz. Once VO_2 is operating in the metallic state, the metamaterial acts as a broadband HWP which has a nearly perfect linear polarization conversion at the frequency range from 3 to 7 THz. Moreover, the metamaterial can play a role of a high-efficiency QWP that can simultaneously convert the incident linear polarized light to left-handed and right-handed circularly polarized light. The calculated ellipticity indicates a good polarization conversion at the frequency of 2.4 THz and 7.4 THz, respectively. The physical mechanism of the above phenomena can be explained by exploring the electric field distributions. Furthermore, the structural parameters also exert great influences for achieving giant CD and HWP as well as QWP. Finally, it should be mentioned that the proposed design is feasible at the current level of fabrication technology. For our presented metamaterials, a sacrificial layer (e.g., Cr layer) can be utilized to obtain a self-contained VO_2–gold-based nanostructure. Firstly, the Cr layer with a thickness of 0.6 μm is deposited on the silicon substrate by using electron beam evaporation (EBA), and then a 0.7 μm VO_2 film is deposited using the magnetron sputtered technique, followed with the deposition of a 0.6 μm Au layer and the spin-coating resist layer (i.e., poly methyl methacrylate (PMMA)). The nanostructure is patterned by using electron beam lithography (EBL) to form the Au split-ring pattern, and then the pattern is transferred into the Au layer through ion beam milling (IBM). Secondly, a SiO_2 layer with the thickness of 9.65 μm is coated on the sample by using EBA to make sure the Au split-ring is well embedded in SiO_2 layer. Next, after stripping the PMMA, the SiO_2 layer is coated on the structure through EBA, followed with the deposition of a 0.7 μm Au layer and a PMMA layer. Thirdly, the nanostructure is patterned by utilizing EBL again to form the upper Au-rod pattern, and then the pattern is transferred into the Au layer with EBL. At last, after stripping the PMMA, the Cr sacrificial layer is removed by Cr etchant, and the final self-contained VO2–gold-based structure is realized. The proposed structure may provide a new approach for developing diversified functional metamaterial devices in THz regions.

Author Contributions: Conceptualization, G.J. and B.T.; methodology, G.J. and Y.R.; software, G.J.; validation, G.J., Y.R. and B.T.; formal analysis, B.T.; investigation, B.T.; resources, G.J.; data curation, G.J.; writing—original draft preparation, G.J., Y.R. and B.T.; writing—review and editing, B.T.; visualization, G.J. and B.T.; supervision, B.T.; project administration, B.T.; funding acquisition, B.T. and G.J. All authors have read and agreed to the published version of the manuscript.

Funding: This research was funded by the Applied Characteristic Disciplines of Electronic Science and Technology of Xiangnan University, and Natural Science Foundation of Jiangsu Province (BK20201446).

Data Availability Statement: The data are included in the main text.

Conflicts of Interest: The authors declare no conflict of interest.

References

1. Cui, Y.; Kang, L.; Lan, S.; Rodrigues, S.; Cai, W. Giant Chiral Optical Response from a Twisted-Arc Metamaterial. *Nano Lett.* **2014**, *14*, 1021–1025. [CrossRef] [PubMed]
2. Huang, Z.; Yao, K.; Su, G.; Ma, W.; Li, L.; Liu, Y.; Zhan, P.; Wang, Z. Graphene-metal hybrid metamaterials for strong and tunable circular dichroism generation. *Opt. Lett.* **2018**, *43*, 2636–2639. [CrossRef] [PubMed]
3. Li, Y.; Dong, G.; Zhao, R.; Wang, K.; Zhou, S.; Sun, L.; Li, P.; Zhu, Z.; Guan, C.; Shi, J. Dual-band asymmetric transmission and circular dichroism in hybrid coupled plasmonic metamaterials. *J. Phys. D Appl. Phys.* **2018**, *51*, 285105. [CrossRef]

4. Ren, Y.; Jiang, C.; Tang, B. Asymmetric transmission in bilayer chiral metasurfaces for both linearly and circularly polarized waves. *JOSA B* **2020**, *37*, 3379–3385. [CrossRef]
5. Tang, B.; Li, Z.; Palacios, E.; Liu, Z.; Butun, S.; Aydin, K. Chiral-Selective Plasmonic Metasurface Absorbers Operating at Visible Frequencies. *IEEE Photon. Tech. Lett.* **2017**, *29*, 295–298. [CrossRef]
6. Rajaei, M.; Zeng, J.; Albooyeh, M.; Kamandi, M.; Hanifeh, M.; Capolino, F.; Wickramasinghe, H.K. Giant Circular Dichroism at Visible Frequencies Enabled by Plasmonic Ramp-Shaped Nanostructures. *ACS Photonics* **2019**, *6*, 924–931. [CrossRef]
7. Huang, Y.; Yao, Z.; Hu, F.; Liu, C.; Yu, L.; Jin, Y.; Xu, X. Tunable circular polarization conversion and asymmetric transmission of planar chiral graphene-metamaterial in terahertz region. *Carbon* **2017**, *119*, 305–313. [CrossRef]
8. Huang, Y.; Xie, X.; Pu, M.; Guo, Y.; Xu, M.; Ma, X.; Li, X.; Luo, X. Dual-Functional Metasurface toward Giant Linear and Circular Dichroism. *Adv. Opt. Mater.* **2020**, *8*, 1902061. [CrossRef]
9. Amin, M.; Siddiqui, O.; Farhat, M. Linear and Circular Dichroism in Graphene-Based Reflectors for Polarization Control. *Phys. Rev. Appl.* **2020**, *13*, 024046. [CrossRef]
10. Xiao, S.; Wang, T.; Liu, T.; Zhou, C.; Jiang, X.; Zhang, J. Active metamaterials and metadevices: A review. *J. Phys. D Appl. Phys.* **2020**, *53*, 503002. [CrossRef]
11. Dănilă, O.; Bărar, A.; Vlădescu, M.; Mănăilă-Maximean, D. An extended k-surface framework for electromagnetic fields in artificial media. *Materials* **2021**, *14*, 7842. [CrossRef] [PubMed]
12. Danila, O.; Manaila-Maximean, D. Bifunctional metamaterials using spatial phase gradient architectures: Generalized reflection and refraction considerations. *Materials* **2021**, *14*, 2201. [CrossRef] [PubMed]
13. Tang, B.; Yang, N.; Song, X.; Jin, G.; Su, J. Triple-band anisotropic perfect absorbers based on α-phase MoO_3 metamaterials in visible frequencies. *Nanomaterials* **2021**, *11*, 2061. [CrossRef]
14. Tang, B.; Guo, Z.; Jin, G. Polarization-controlled and symmetry-dependent multiple plasmon-induced transparency in graphene-based metasurfaces. *Opt. Express* **2022**, *30*, 35554–35566. [CrossRef]
15. Grady, N.K.; Heyes, J.E.; Chowdhury, D.R.; Zeng, Y.; Reiten, M.T.; Azad, A.K.; Taylor, A.J.; Dalvit, D.A.; Chen, H.-T. Terahertz metamaterials for linear polarization conversion and anomalous refraction. *Science* **2013**, *340*, 1304–1307. [CrossRef]
16. Yu, Y.; Xiao, F.; He, C.; Jin, R.; Zhu, W. Double-arrow metasurface for dual-band and dual-mode polarization conversion. *Opt. Express* **2020**, *28*, 11797–11805. [CrossRef] [PubMed]
17. Azzam, R.M.A.; Bashara, N.M. *Ellipsometry and Polarized Light*; North-Holland: New Yourk, NY, USA, 1977.
18. Zheng, Q.; Guo, C.; Ding, J. Wideband Metasurface-Based Reflective Polarization Converter for Linear-to-Linear and Linear-to-Circular Polarization Conversion. *IEEE Antennas Wirel. Propag. Lett.* **2018**, *17*, 1459–1463. [CrossRef]
19. Wu, P.C.; Sokhoyan, R.; Shirmanesh, G.K.; Cheng, W.-H.; Atwater, H.A. Near-Infrared Active Metasurface for Dynamic Polarization Conversion. *Adv. Opt. Mater.* **2021**, *9*, 2100230. [CrossRef]
20. Zhang, Y.; Feng, Y.; Zhao, J. Graphene-enabled tunable multifunctional metamaterial for dynamical polarization manipulation of broadband terahertz wave. *Carbon* **2020**, *163*, 244–252. [CrossRef]
21. Jia, Z.; Huang, L.; Su, J.; Tang, B. Tunable electromagnetically induced transparency-like in graphene metasurfaces and its application as a refractive index sensor. *J. Lightwave Technol.* **2021**, *39*, 1544–1549. [CrossRef]
22. Zhu, Y.; Tang, B.; Jiang, C. Tunable ultra-broadband anisotropic absorbers based on multi-layer black phosphorus ribbons. *Appl. Phys. Express* **2019**, *12*, 032009. [CrossRef]
23. Quader, S.; Zhang, J.; Akram, M.R.; Zhu, W. Graphene-based high-efficiency broadband tunable linear-to-circular polarization converter for terahertz waves. *IEEE J. Sel. Top. Quantum Electron.* **2020**, *26*, 1–8. [CrossRef]
24. Park, J.; Kang, J.-H.; Kim, S.J.; Liu, X.; Brongersma, M.L. Dynamic reflection phase and polarization control in metasurfaces. *Nano Lett.* **2017**, *17*, 407–413. [CrossRef] [PubMed]
25. Liu, H.; Lu, J.; Wang, X.R. Metamaterials based on the phase transition of VO_2. *Nanotechnology* **2017**, *29*, 24002. [CrossRef]
26. Kocer, H.; Butun, S.; Ba Nar, B.; Wang, K.; Tongay, S.; Wu, J.; Aydin, K. Thermal tuning of infrared resonant absorbers based on hybrid gold-VO2 nanostructures. *Appl. Phys. Lett.* **2015**, *106*, 161104. [CrossRef]
27. Lei, L.; Lou, F.; Tao, K.; Huang, H.; Cheng, X.; Xu, P. Tunable and scalable broadband metamaterial absorber involving VO_2-based phase transition. *Photon. Res.* **2019**, *7*, 734–741. [CrossRef]
28. Ren, Y.; Zhou, T.; Jiang, C.; Tang, B. Thermally switching between perfect absorber and asymmetric transmission in vanadium dioxide-assisted metamaterials. *Opt. Express* **2021**, *29*, 7666–7679. [CrossRef]
29. Wang, T.; Zhang, H.; Zhang, Y.; Zhang, Y.; Cao, M. Tunable bifunctional terahertz metamaterial device based on Dirac semimetals and vanadium dioxide. *Opt. Express* **2020**, *28*, 17434–17448. [CrossRef]
30. Song, Z.; Zhang, J. Achieving broadband absorption and polarization conversion with a vanadium dioxide metasurface in the same terahertz frequencies. *Opt. Express* **2020**, *28*, 12487–12497. [CrossRef]
31. Yan, D.; Meng, M.; Li, J.; Li, J.; Li, X. Vanadium dioxide-assisted broadband absorption and linear-to-circular polarization conversion based on a single metasurface design for the terahertz wave. *Opt. Express* **2020**, *28*, 29843–29854. [CrossRef]
32. Zhang, J.; Zhang, K.; Cao, A.; Liu, Y.; Kong, W. Bi-functional switchable broadband terahertz polarization converter based on a hybrid graphene-metal metasurface. *Opt. Express* **2020**, *28*, 26102–26110. [CrossRef] [PubMed]
33. Mao, M.; Liang, Y.; Liang, R.; Zhao, L.; Xu, N.; Guo, J.; Wang, F.; Meng, H.; Liu, H.; Wei, Z. Dynamically Temperature-Voltage Controlled Multifunctional Device Based on VO_2 and Graphene Hybrid Metamaterials: Perfect Absorber and Highly Efficient Polarization Converter. *Nanomaterials* **2019**, *9*, 1101. [CrossRef] [PubMed]

34. Ren, Y.; Tang, B. Switchable Multi-Functional VO_2-Integrated Metamaterial Devices in the Terahertz Region. *J. Lightwave Technol.* **2021**, *39*, 5864–5868. [CrossRef]
35. Wang, R.; Tang, B. Tri-functional metamaterials integrated with vanadium dioxide in terahertz regions. *Phys. E Low-Dimens. Syst. Nanostructures* **2022**, *144*, 115414. [CrossRef]
36. Qi, H.; Tang, B. Active tunable terahertz functional metamaterial based on hybrid-graphene vanadium dioxide. *Phys. Chem. Chem. Phys.* **2023**. [CrossRef] [PubMed]
37. Ding, F.; Zhong, S.; Bozhevolnyi, S.I. Vanadium Dioxide Integrated Metasurfaces with Switchable Functionalities at Terahertz Frequencies. *Adv. Opt. Mater.* **2018**, *6*, 1701204. [CrossRef]
38. Luo, J.; Shi, X.; Luo, X.; Hu, F.; Li, G. Broadband switchable terahertz half-/quarter-wave plate based on metal-VO_2 metamaterials. *Opt. Express* **2020**, *28*, 30861–30870. [CrossRef]
39. Tang, B.; Ren, Y. Tunable and switchable multi-functional terahertz metamaterials based on a hybrid vanadium dioxide–graphene integrated configuration. *Phys. Chem. Chem. Phys.* **2022**, *24*, 8408–8414. [CrossRef]
40. Zhao, J.; Song, J.; Xu, T.; Yang, T.; Zhou, J. Controllable linear asymmetric transmission and perfect polarization conversion in a terahertz hybrid metal-graphene metasurface. *Opt. Express* **2019**, *27*, 9773–9781. [CrossRef]

Disclaimer/Publisher's Note: The statements, opinions and data contained in all publications are solely those of the individual author(s) and contributor(s) and not of MDPI and/or the editor(s). MDPI and/or the editor(s) disclaim responsibility for any injury to people or property resulting from any ideas, methods, instructions or products referred to in the content.